ON PROBABILISTIC DESIGN OF A CONCRETE FLOATING BRIDGE

Bernt J. Leira
SINTEF, Division of Structural Engineering, Trondheim,
Research Engineer.

Ivar Langen
SINTEF, Division of Structural Engineering, Trondheim,
Senior Research Engineer.

Three different design alternatives of a concrete floating bridge are compared by means of the Hasofer-Lind index. The reliability level is also evaluated by means of an outcrossing rate method, and the influence of prestressing force is assessed.

Keywords: Concrete floating bridge, limit states, reliability measures.

1. INTRODUCTION

The floating bridge structural concept has attracted more and more attention in Norway during the last years. This is especially the case for bridging the widest and deepest fjords on the western coast, where more traditional designs will be very costly. Thus, after some years of planning, the Norwegian Government has proposed to build a bridge of this type across the fjord at Salhus outside Bergen /1/.

This bridge is of the continuous pontoon type with a curved box pontoon of prestressed concrete supporting the bridge deck. Other bridges of the same kind has been in operation in the State of Washington, U.S.A., for several years. Among them is the well-known Hood Canal Bridge which was completed in 1961 and is located near the Olympic Peninsula.

Common for bridges of this type is that the pontoon pierces the water surface and therefore is exposed to large wave forces, and also current and static wind forces may be significant. The severity of the environmental

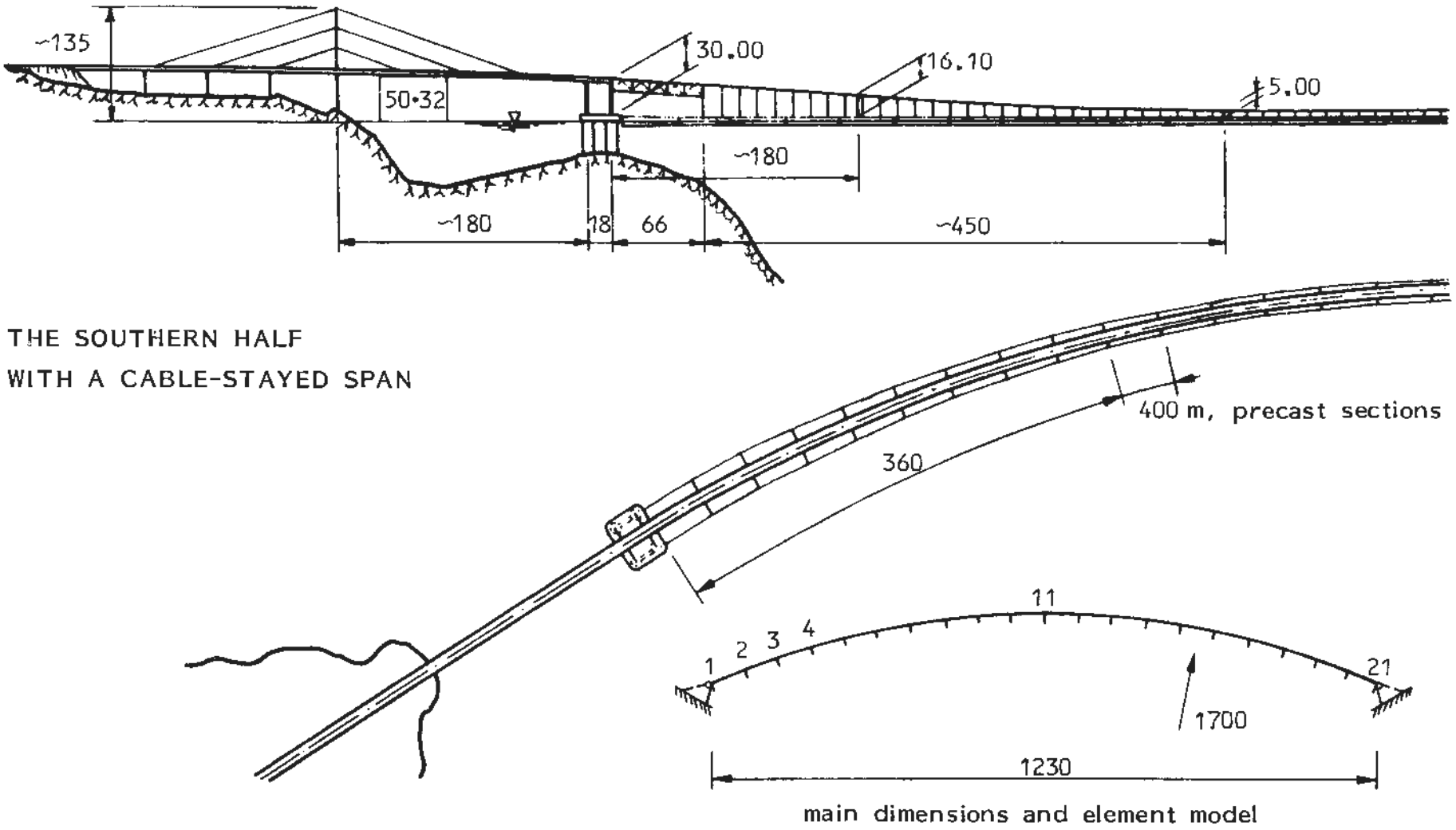

Figure 1 The Salhus floating bridge - dimensions in m

forces is underlined by the Hood Canal Bridge disaster on the 13th of February, 1979 /2,3,4/.

Therefore, it seems to be of vital importance to predict the safety level of these bridges. This requires not only reliable models of load and load effects, but also models for stochastic dynamic response analysis. In addition the different limit states must be defined, and proper safety measures introduced and computed.

Dynamic analysis of floating bridges and similar structures has been treated in the literature by several authors, see for instance references /4-12/. Also, in Reference /13/ safety against collapse for the serviceability limit state of a bridge cross-section is evaluated by means of the Hasofer-Lind index.

This paper deals both with the theoretical analysis of the wave induced vibrations of floating bridges and the computation of safety against collapse for two different limit states. A comparison of three different design alternatives is achieved by means of the Hasofer-Lind β-index, and furthermore the influence of prestress force upon this index is studied. Secondly, a more correct reliability analysis is carried out by a so-called outcrossing rate method where the response is modelled as a stochastic vector process. Thus, the corresponding probability of failure may be estimated for a design storm of given duration, and also in a long term sense whenever wave data are available. The proposed Salhus floating bridge serves as an example structure.

2. THE SALHUS BRIDGE PROJECT

The bridge is designed as a horizontal arch, consisting of a 1200 metres long continuous, curved concrete pontoon floating on the sea surface, see Fig. 1. the pontoon supports the roadway concrete slab by means of columns ranging in height from 5.5 metres to 28 metres. Watertight bulkheads are provided within the pontoon units for the dual purpose of limiting compartment size for damage control and of supporting the superstructure.

In this paper, three different designs are considered. Two of these have identical geometric characteristics and differ only by the amount of steel reinforcements. The geometric data of the two alternative bridge mid-

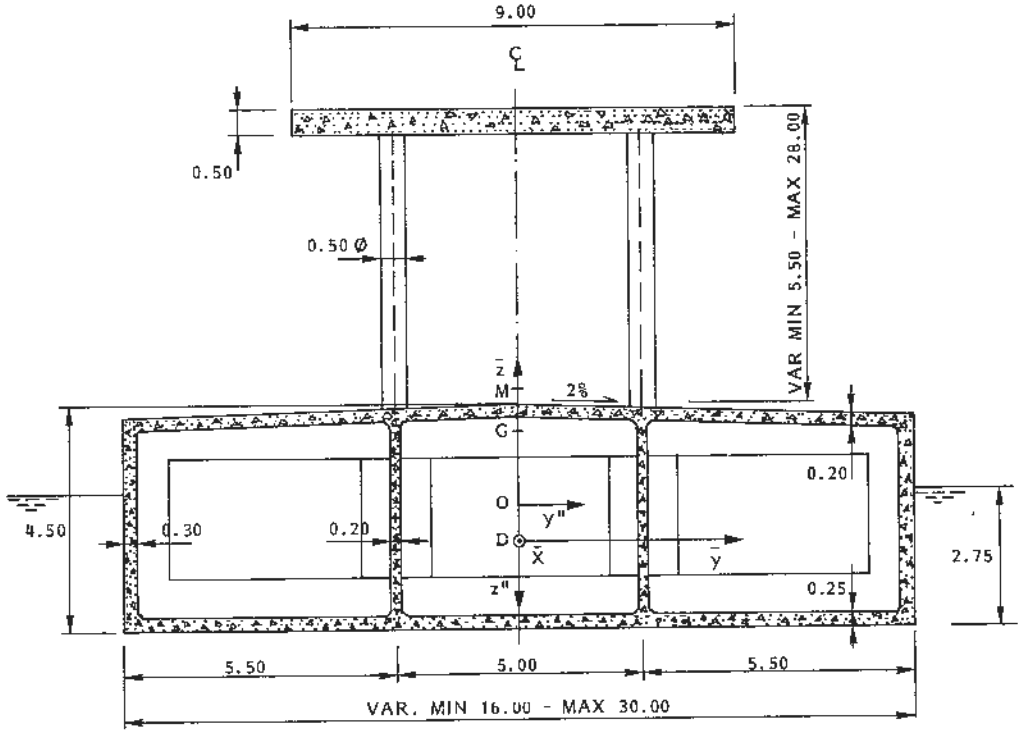

(a) Design alternatives 1 and 2

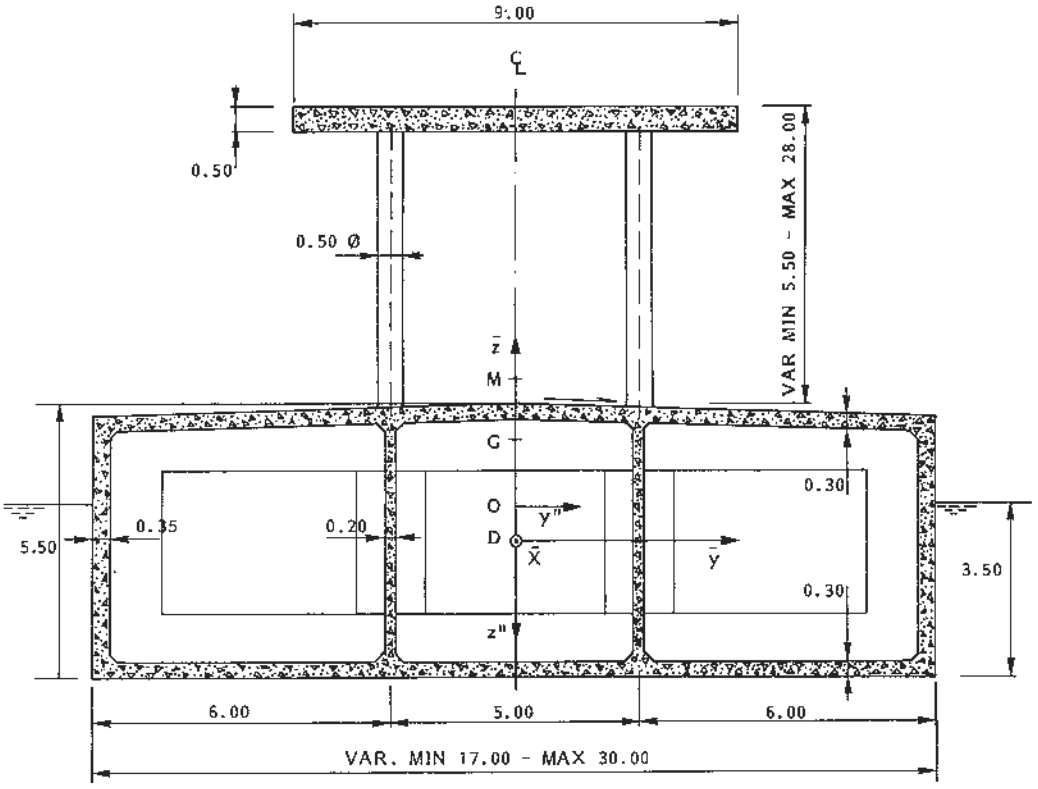

(b) Design alternative 3

Figur 2 Geometric data for the three alternative bridge designs. Dimensions in m

sections are displayed in Fig. 2. The given minimum dimensions are used except at the southern end. Here the slab is raised and connected to a cable-stayed bridge span to allow sufficient free sailing space, see Fig. 1. The number of cells (three in Fig. 2) is increased to maximum 7 at the southern end.

Hinge sections are implemented at the ends to allow the bridge to follow the tide variations. Anchoring of this bridge is not feasible due to the deep fjord conditions. Therefore lateral forces from waves, current and wind have to be balanced by bending, torque and axial forces in the pontoon itself.

3. RESPONSE ANALYSIS

The structure is modelled according to the finite element method by 20 beam elements with appropriate boundary conditions at the bridge ends, see Fig. 1. The equation of motion may be written

$$M^{(s)}\,\ddot{r}(t) + C^{(s)}\,\dot{r}(t) + K^{(s)}\,r(t) = Q^{(h)}(t) \qquad (1)$$

in which $M^{(s)}$, $C^{(s)}$ and $K^{(s)}$ are the structural mass, damping and stiffness matrices; $r(t)$ is a vector of nodal displacement parameters consisting of three translational and three rotational components at each node; and $Q^{(h)}(t)$ is the corresponding hydrostatic and hydrodynamic load vector.

In the short term sea state model employed, the sea elevation is described as a zero mean, ergodic Gaussian field. This implies that the sea is completely described by second order statistics which is here expressed in terms of the cross spectral density as

$$S_{\eta_m \eta_n}(\omega) = S_\eta(\omega) \int_\theta \psi(\theta) \cdot \exp\{-i\,\mathrm{sign}(\omega)\,\kappa(\omega) \cdot ((x_m - x_n)\cos\theta + (y_m - y_n)\sin\theta)\}d\theta \qquad (2)$$

where η_m denotes the sea elevation at position $x_m = [x_m, y_m]^T$ in the mean sea surface horizontal plane; ω is the circular frequency; $\kappa(\omega)$ is the scalar wave number; i is the imaginary unit; θ is the wave propagation direction; $S_\eta(\omega)$ is the one-dimensional wave spectral density; and $\psi(\theta)$ is the spreading function commonly assumed to be frequency independent.

The spreading function used is a general cosine function of the type

$$\psi(\theta) = C \cos^n(\theta-\bar{\theta}) \qquad -\frac{\pi}{2} < \theta - \bar{\theta} \leq \frac{\pi}{2} \tag{3}$$

where n is a parameter defining the width of the distribution; $\bar{\theta}$ denotes the average direction of wave propagation and C is a normalization factor defined so that the integral of the spreading function between $-\frac{\pi}{2}$ and $\frac{\pi}{2}$ is one.

The spectral density matrix $S_Q(\omega)$ of the nodal point wave excitation vector $Q(t)$ may be expressed by the one-dimensional wave spectral density as

$$S_Q(\omega) = F(\omega)\ S_\eta(\omega) \tag{4}$$

where $F(\omega)$ is the hydrodynamic transfer function. $F(\omega)$ is a Hermitian matrix taking care of the kinematics and the spatial structure of the wave field and the wave loading mechanism. The calculation of the wave loading on the bridge is based on linear potential theory and two-dimensional flow in combination with a strip theory /15,16/.

The virtual frequency response function of the fluid-structure system given as

$$H(\omega) = [K - \omega^2 M(\omega) + i\omega C(\omega)]^{-1} \tag{5}$$

may then be introduced. Here, K is now the stiffness matrix including hydrostatic restoring. $M(\omega)$ is the mass matrix including a frequency dependent hydrodynamic mass; and $C(\omega)$ is the damping matrix, which is predominated by the hydrodynamic damping terms. The spectral density matrix of the structural response processes is then readily expressed as

$$S_r(\omega) = H(\omega)\ S_Q(\omega)\ H^{*T}(\omega) = B(\omega)\ S_\eta(\omega) \tag{6}$$

where $H^{*T}(\omega)$ denotes the complex conjugate and transposed matrix of $H(\omega)$. The matrix

$$B(\omega) = H(\omega)\ F(\omega)\ H^{*T}(\omega) \tag{7}$$

denotes the transfer function of the structure-fluid system relating the response spectral density matrix to the wave spectral density.

The force (or stress) spectral densities are derived by means of a real and frequency independent matrix E:

$$S_R(\omega) = E\, S_r(\omega)\, E^T \tag{8}$$

The cross-correlation coefficients $\rho_{R_iR_i}$ between response quantities R_i and R_j may be evaluated from this spectral matrix. Similarly, the cross-correlation coefficients of the velocity processes, $\rho_{\dot{R}_i\dot{R}_j}$ and $\rho_{R_i\dot{R}_j}$, are derived by well-known relationships, /25/.

4. RELIABILITY MEASURES

4.1 The Hasofer-Lind index

Detailed descriptions of the computation and interpretation of the Hasofer-Lind β-index are found elsewhere, e.g. references /17,18,19/. The starting point is a set of n basic random variables $\mathbf{x} = [x_1, x_2, \ldots. x_n]^T$. These are chosen in such a way that the failure surface can be defined in the n-dimensional basic variable space Ω. This surface is given by the equation

$$f(\mathbf{x}) = f(x_1, x_2, x_3, \ldots, x_n) = 0 \tag{9}$$

where positive values of the failure function f indicate the safe region Ω_S and negative values the failure region Ω_f:

$$\begin{aligned} f(\mathbf{x}) &> 0 \quad \text{when} \quad \mathbf{x} \in \Omega_s \\ &\leqslant 0 \quad \text{when} \quad \mathbf{x} \in \Omega_f \end{aligned}$$

Corresponding to the basic variables the expectation vector μ_x and the correlation matrix are given:

$$\begin{aligned} \mu_x &= [\mu_1, \mu_2, \ldots, \mu_n]^T \\ C_x &= E\{x^T x\} - \mu_x^T \mu_x \end{aligned} \tag{10}$$

where $E\{\cdot\}$ denotes the expectation operator.

Evaluation of the Hasofer-Lind index now requires a transformation of the basic variables into a new set of uncorrelated and normalized variables $\mathbf{z} = [z_1, z_2, \ldots, z_n]^T$. This transformation may be expressed as

$$z = A\, x \tag{11}$$

where **A** depends on the eigenvectors and eigenvalues of matrix C_x. Similarly, the failure surface is also transformed into a failure surface, $\delta\Omega_z$, in normalized space given by the equation

$$g(\mathbf{z}) = g(z_1, z_2, \ldots, z_n) = 0 \qquad (12)$$

The Hasofer-Lind reliability index, β, is now defined as the shortest distance from the origin to the limit state surface:

$$\beta = \min_{\mathbf{z} \in \partial\Omega_z} (\mathbf{z}^T \mathbf{z})^{\frac{1}{2}}$$

A flow chart of a computer program for computation of this index in the case of nonlinear failure surfaces is included in Reference /20/.

It should be noted that the β-index assumes the basic quantities to be random variables rather than stochastic processes. Thus, the duration of the process and the properties of the velocities are disregarded. A more correct approach would be to start with the distribution of maxima of the vector component processes and then apply the so-called Rosenblatt transformation, /18/. Then the computation of the β-index as defined above may be carried out. A serious problem with this procedure, however, is the lack of knowledge about the joint distribution of maxima for the vector components and thereby crosscorrelations of maxima.

Thus, it seems that a correct representation in the case of basic process components is only possible within a level 3 framework as described in the next section.

4.2 The outcrossing rate and probability of failure

The basic variables above are now instead regarded as components of a stochastic vector process

$$\mathbf{x}(t) = [x_1(t), x_2(t), \ldots, x_n(t)]^T$$

which should stay within the safe region Ω_s bounded by the failure surface. Usually there is a non-zero probability of this process to outcross Ω_s into

the failure region Ω_s during a reference time interval T. The multidimensional generalization of the formula for the outcrossing rate is expressed as

$$\nu_{\Omega_s} = \int_{\partial\Omega_x} \int_0^\infty \dot{x}_n \, f_{X,\dot{X}_n}(x,\dot{x}_n) d\dot{x}_n \, dx \tag{13}$$

see References /13,21,22,23/. Here, $\dot{x}_n$ is the velocity normal to the failure surface Ω_s; and $f_{X,\dot{X}_n}(\cdot)$ is the joint probability density function of x and $\dot{x}_n$. After transformation into normalized space as described in the previous section, this expression becomes

$$\nu_{\Omega_s} = \int_{\partial\Omega_z} \int_0^\infty \dot{z}_n \, f_{Z,\dot{Z}_n}(z,\dot{z}_n) d\dot{z}_n \, dz \tag{14}$$

where $f_{Z,\dot{Z}_n}(z,\dot{z}_n)$ is defined analoguously to above.

In the case that $\mathbf{x}(t)$ contains both process components $\mathbf{x}_p(t)$ and ordinary stochastic variables x_v a partitioning is possible:

$$\begin{aligned} x(t) &= [x_p(t),\, x_v]^T \\ &= [x_1(t),\, x_2(t) \ldots x_k(t),\, x_{k+1} \ldots x_n]^T \end{aligned} \tag{15}$$

The outcrossing rate may now be found by conditioning:

$$\nu_{\Omega_s} = \int_{x_v} \int_{\partial\Omega_{x|x_v}} \int_0^\infty \dot{x}_{n_p} \, f_{X_p,\dot{X}_{n_p}|x_v}(x_p,\dot{x}_{n_p}|x_v) d\dot{x}_{n_p} \, d(\partial\Omega_{x|x_v}) \cdot g_{X_v}(x_v) \, dx_v \tag{16}$$

which in the case of no correlation between $x_p(t)$ and x_v becomes

$$\nu_{\Omega_s} = \int_{x_v} \int_{\partial\Omega_{x|x_v}} \left\{ \int_0^\infty \dot{x}_{n_p} \, f_{X_p,\dot{X}_{n_p}}(x_p,\dot{x}_{n_p}) d\dot{x}_{n_p} \right\} d(\partial\Omega_{x|x_v}) \cdot g_{X_v}(x_v) \, dx_v \tag{17}$$

Above, $\partial\Omega_{x|x_v}$, is the failure surface for given values of the x_v

components; $\dot{x}_{n_p}$ is the normal velocity to this "restricted surface"; $f_{\mathbf{X}_p,\dot{X}_{n_p}|\mathbf{X}_v}(\mathbf{x}_p,\dot{x}_{n_p}|\mathbf{x}_v)$ is the joint probability density function of $\mathbf{x}_p$ and $\dot{x}_{n_p}$ for given values of $\mathbf{x}_v$; and $g_{\mathbf{X}_v}(\mathbf{x}_v)$ is the joint density of the $\mathbf{x}_v$ components. Similar expressions to Eqs. (16), (17) also hold for the transformed variables $\mathbf{z}$.

The evaluation of the double integral in Eqs. (13), (14) and the inner part of Eqs. (16), (17) can only be computed analytically for a limited number of cases. A collection of such formulaes may be found in Reference /23/ for the special case of a diagonal covariance matrix and Gaussian processes. In the sequel, a two-dimensional outcrossing rate formulation will be considered where the covariance matrix is fully populated:

$$\mathbf{C}_{\mathbf{x}_p\dot{\mathbf{x}}_p} = \begin{bmatrix} \sigma^2_{x_1} & \rho_1\sigma_{x_1}\sigma_{x_2} & 0 & \rho_3\sigma_{x_1}\sigma_{\dot{x}_2} \\ \text{Symm.} & \sigma^2_{x_2} & \rho_2\sigma_{x_2}\sigma_{\dot{x}_1} & 0 \\ & & \sigma^2_{\dot{x}_1} & \rho_4\sigma_{\dot{x}_1}\sigma_{\dot{x}_2} \\ \text{Symm.} & & \text{Symm.} & \sigma^2_{\dot{x}_2} \end{bmatrix} \tag{18}$$

Here, ρ_1, ρ_2, ρ_3, ρ_4 are four different correlation coefficients, among which ρ_2 and ρ_3 are related by

$$\rho_2\sigma_{x_2}\sigma_{\dot{x}_1} = -\rho_3\sigma_{x_1}\sigma_{\dot{x}_2} \tag{19}$$

After transformation, the covariance matrix $\mathbf{C}_{\mathbf{Z}_p\dot{\mathbf{Z}}_p}$ will have the shape

$$\mathbf{C}_{\mathbf{Z}_p\dot{\mathbf{Z}}_p} = \begin{bmatrix} 1 & 0 & 0 & s\sigma_{\dot{z}_2} \\ 0 & 1 & r\sigma_{\dot{z}_1} & 0 \\ \text{Symm.} & & \sigma^2_{\dot{z}_1} & t\sigma_{\dot{z}_1}\sigma_{\dot{z}_2} \\ & & \text{Symm.} & \sigma^2_{\dot{z}_2} \end{bmatrix} \tag{20}$$

where $r\sigma_{\dot{z}_1} = -s\sigma_{\dot{z}_2}$.

A general two-dimensional failure surface may be closely approximated by a sequence of straight line segments. As the number of segments increases, the accuracy of this approximation can be made to increase. In Reference /24/ an analytical expression for the outcrossing rate for a straight line segment Δs in the general case of the covariance matrix (25) is developed for a Gaussian vector process. This expression is of the form

$$\nu_{\Delta s} = c_1 e^{-\frac{1}{2}R^2} \left[\Phi\{\alpha\xi\}\right]_{\xi_l}^{\xi_u} + c_2\, r e^{-\frac{1}{2}R^2} \left[\Phi\{\beta\xi\} e^{-\frac{1}{2}\xi^2}\right]_{\xi_l}^{\xi_u} \tag{21}$$

Here c_1, c_2, α and β are constants; ξ is a local coordinate for the line segment, and ξ_u, ξ_l are corresponding upper and lower values for the segment end points; R^2 is the distance from the segment line to the origin; and $\Phi\{\cdot\}$ is the standard normal distribution function. By setting $r = t = s = 0$ above, both matrix (20) and expression (21) degenerate into expressions given in Reference /23/. The outcrossing rate for the failure surface is finally found by summing contributions from all line segments.

When the outcrossing rate is computed, close bounds on the probability of failure during a time interval T may be obtained from the expressions, /23/:

$$p_f(T) \leq p_f(o) + [1 - p_f(o)]\nu_{\Omega_s} T \tag{22}$$

or

$$p_f(T) = 1 - [1 - p_f(o)]e^{-\nu_{\Omega_s} T} \tag{23}$$

where (23) is based on the assumption of Poisson exits out of the safe region; and $p_f(o)$ is the initial probability of failure at time $t = 0$.

5. FAILURE SURFACES

5.1 General

A typical example of variation of maxima of bending moments M_y and M_z along the bridge span is shown in Fig. 3 (see Ref. /15/). Also the variation of the correlation coefficient between the bending moments is displayed, and it can be concluded that the most critical cross-section will be close to the mid-section of the bridge. This is due to the high absolute value of the correlation coefficient at this point, which implies that large values of the bending moments will tend to occur simultaneously.

In the following, collapse criteria for the mid-section will be studied in some detail, and in a simplified system analysis this collapse may also be taken as the system failure mode.

5.2 Serviceability limit state

The criterion applied for this limit state is initial cracking of concrete at the mid-section. The tensile stress capacity of concrete is put equal to zero, and cracking will thus take place when the tensile stresses due to the bending moments exceed the compressive pretension stress. The safe region is then defined by the inequality, /13/:

$$f(P_k, M_y, M_z) =$$

$$\frac{1}{A'_c}\left(\sum_k P_k + N\right) + \left[\frac{1}{I'_y}\sum_k P_k z_k + \frac{M_y}{I_y}\right]z$$

$$+ \left[\frac{1}{I'_z}\sum_k P_k y_k + \frac{M_z}{I_z}\right]y \geq 0 \qquad (24)$$

where P_k, M_y and M_z are respectively the prestress in cable number k, the bending moments about the y-axis and about the z-axis; N is the additional axial force acting on the cross section; A'_c is the area of the transformed cross-section; I_z and I'_z are the moments of inertia about the z-axis of the transformed cross-section with and without prestressing steel; I_y and I'_y are the corresponding moments of inertia about the y-axis; z_k and y_k are the coordinates of the prestressing cable positions, and z,y are the coordinates of the desired cross-section point. Further explanations are found in Reference /13/. As a first simplification

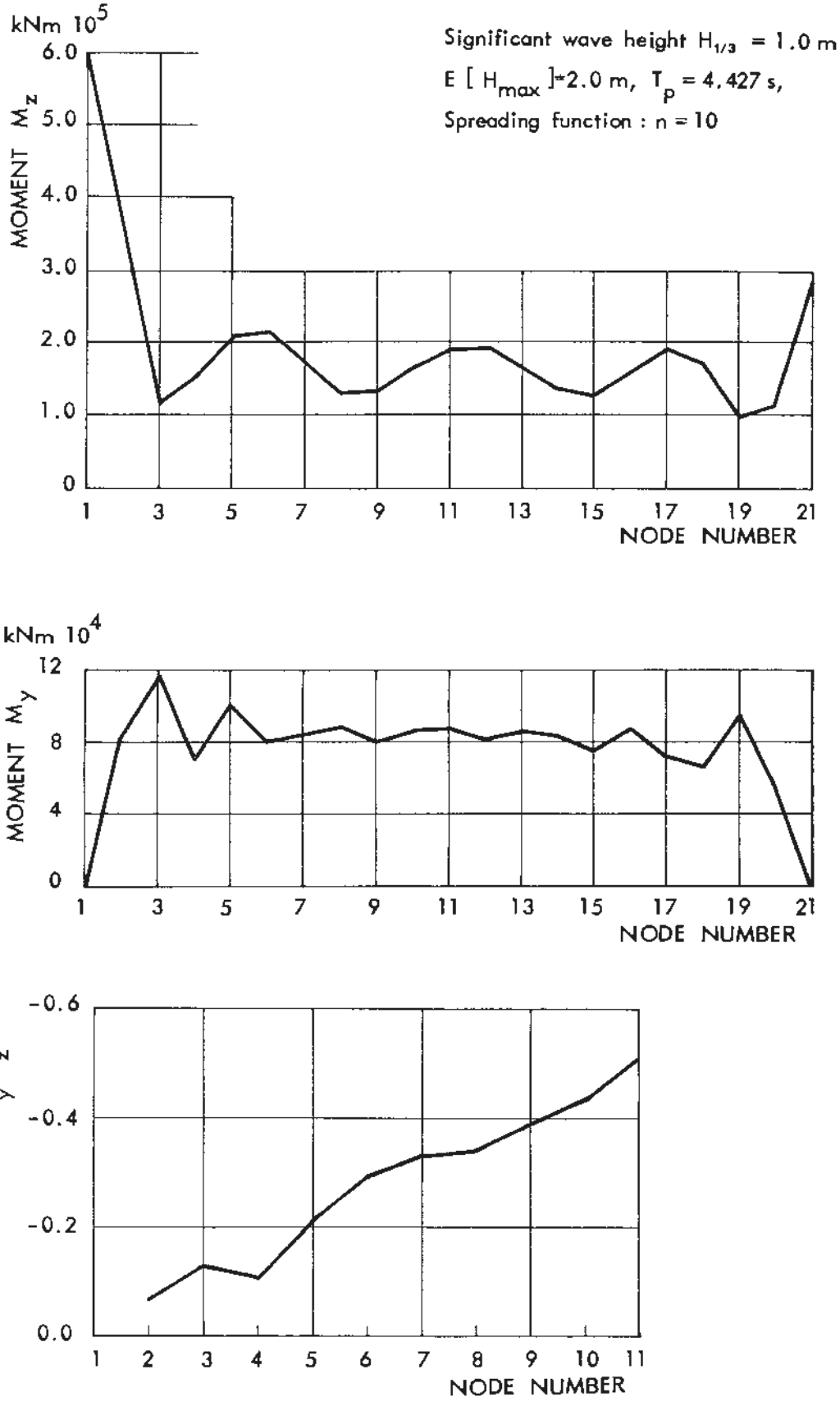

Figure 3 Example of variation of maxima of bending moments and correlation coefficient. Design alternative 1

A'_c, I_z, I'_z, I_y and I'_y may be regarded as constants. The effect of including them among the variables with typical expectation values and variances is not very significant, /25/.

A maximum limit on the level of axial force must also be introduced. According to the Norwegian design code, /26/, this limit depends on the quality of concrete. Here, however, this limit is simply taken to be 75% of the maximum axial load for the ultimate limit state.

The bending moments above will generally be correlated stochastic processes, and correspond to the vector $x_p(t)$ in section 4.2, while the axial force may be regarded as a simple stochastic variable in a short term analysis and corresponds to vector x_v above.

5.3 Ultimate limit state

This limit state is defined as total collapse of the mid-section, and it is defined in terms of permissible concrete and steel strains. According to Reference /27/, the limit strains are taken as $\varepsilon_{c,max} = 3.5$ o/oo for both the concrete and the steel reinforcement in compression. The maximum steel reinforcement tensile strain is $\varepsilon_{sy} + 5$ o/oo where ε_{sy} is the strain at initial yielding. The assumed strain variation across the section is also explained in Reference /27/. The values of the corresponding equilibrated axial force and bending moments are computed by means of numerical iteration. The procedure is implemented in a computer program and may shortly be described as follows, /27/:

1. step: Choose direction of neutral axis passing through the shear center. Specify magnitude of the total axial force acting on the cross-section.

2. step: Compute internal axial forces corresponding to the two extreme permissible strain states. Now apply the secant method, /28/, and iterate on strain state until equilibrium of external and internal axial force is obtained.

3. step: Compute bending moments corresponding to said strain state.

Each set of three force resultants yields one point in (M_y, M_z, P)-space, and the collection of all such points will describe the failure surface.

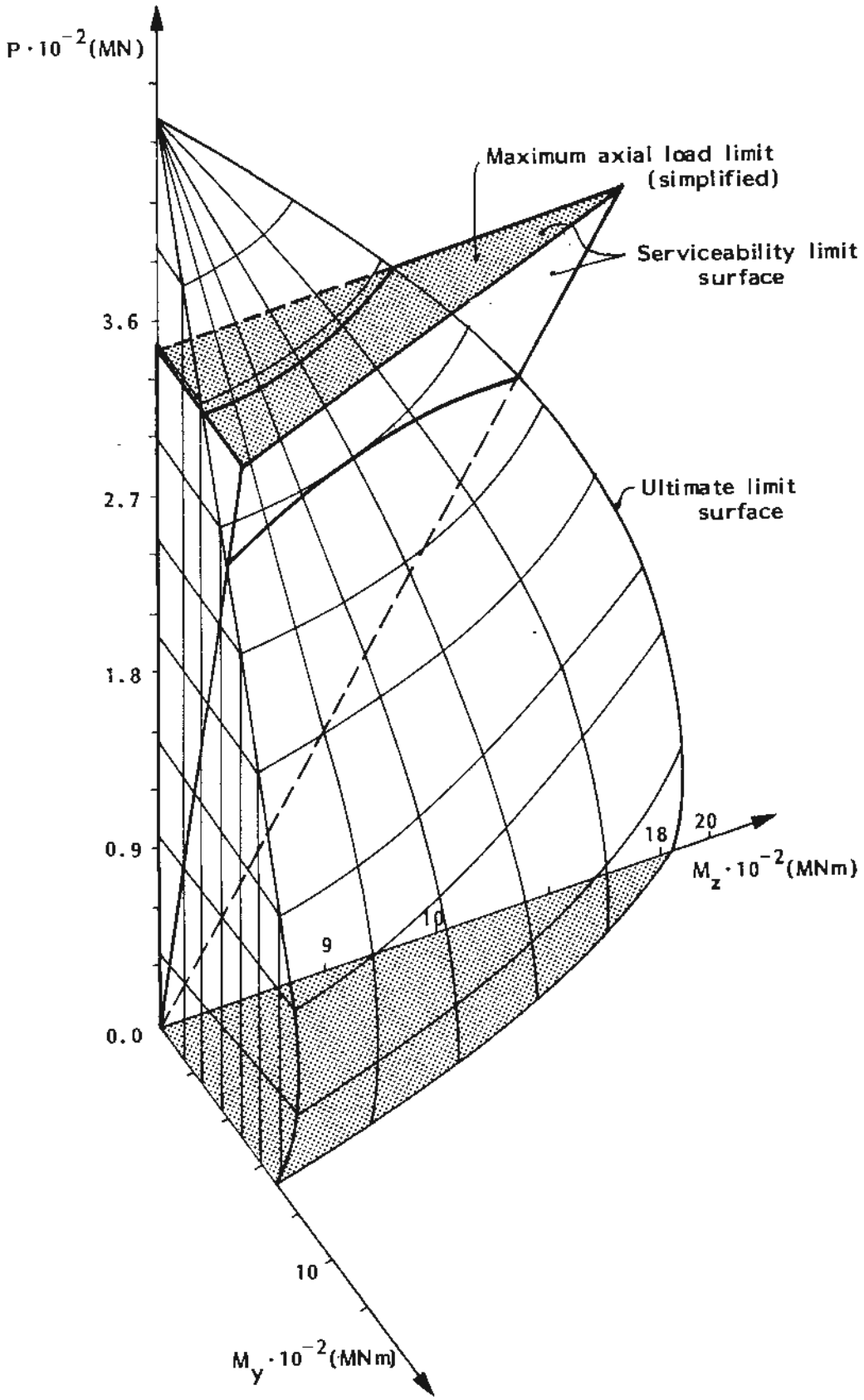

Figure 4 Failure surfaces in basic variable space. Redrawn from Refs. /20, 25/

An example of a serviceability failure surface and a corresponding ultimate failure surface is displayed in Figure 4. Only the first octant is shown, and smooth curves are drawn through the discrete set of points for the sake of appearance. These surfaces will be symmetric about the M_y-P and the M_z-P plane. The serviceability failure surface will have its "bottom point" at the origin of the M_z - M_y plane, while the ultimate failure surface will have a "shallow" extension below this plane.

For evaluation of the β-index defined above it will be more convenient with an analytical expression defining the ultimate failure surface than a numerical description. A suitable expression approximating the surface satisfactorily is a quadratic form:

$$f(M_y,M_z,P) = C_1 + C_2P + C_3P^2 + C_4M_y + C_5M_y^2 + C_6M_z + C_7M_yP^2 \qquad (25)$$

where the constants C_1, C_2, C_3, C_4, C_5, C_6 and C_7 are recomputed for each failure surface.

It should also be noted that the axial force P above includes both the prestress and the additional axial forces N:

$$P = \sum_k P_k + N \qquad (26)$$

6. RESULTS

Dynamic response analyses have been carried out for the three different bridge design alternatives in Section 2 above. The geometric data of the mid-sections are displayed in Figure 2, and the first design alternative is the one previously analysed in References /13,15,16/. This design may be regarded as the "lightest and softest", and the stiffness characteristics employed do not include the effect of any slack steel reinforcements. The second variant is identical except for the recomputation of cross-sectional constants to include the effect of steel reinforcements according to the data from Reference /29/. The third design is the "heaviest and stiffest" one, and has a minimum width of 17 metres. Further details are found in References /20,25/.

The wave environment of the analyses is described by a Jonswap spectrum with significant wave height H_S = 1.0, peakedness parameter γ = 7.0 and

peak period T_p = 6.0s. The short-crestedness of the waves is represented by a cosine-type spreading function with exponent n = 2, i.e. extremely short-crested waves.

Table 1 displays the variances and covariances of the moments at the mid-section for the three alternative designs. Also the expected largest responses for a stationary sea state duration of 0.1 hr and 2.0 hrs are included. It is found that the variation of bending moments and correlation coefficients along the bridge span is quite similar for the three alternatives. However, as seen from Table 1 the magnitude of the correlation coefficient at the mid-section will vary considerably between designs.

Table 1 Statistical properties of response bending moments at mid-section

Statistical quantity		Alternative number		
		1	2	3
σ_{M_z} [MNm]		22.53	23.96	23.81
σ_{M_z} [MNm]		80.73	85.62	75.80
$\rho(M_y, M_z)$		- 0.49	- 0.49	- 0.39
$E[(M_y)_{max}]$ [MNm]	ΔT = 0.1 hr	69.24	73.66	73.29
	ΔT = 2.0 hrs	88.48	94.10	93.59
$E[(M_z)_{max}]$ [MNm]	ΔT = 0.1 hr	245.7	262.1	233.4
	ΔT = 2.0 hrs	314.6	335.4	298.0

For the purpose of comparing the different designs and studying the influence of prestress level on the bridge capacity, the β-index as described in section 4.1 above is a convenient measure. Bearing in mind the limitations of this index as already described, it will still represent the correlation and variability of the loading in a correct manner.

It should be noted that in advance, it is not reasonable to expect a monotonous increase in safety level with increasing stiffness characteristics with respect to wave loads. This is due to redistribution of internal forces and changes in correlation magnitude implied by stiffness alterations. Also, a possible increase of outer dimensions of the pontoon may increase the hydrodynamic coefficients and thereby the loads.

The stochastic variation of prestressing force is taken as uncorrelated with the bending moments for a short term sea state. The coefficients of variation are taken as $CV[P_K] = 10\%$ and $CV[P_K] = 15\%$ for the prestress in the cables above and below the mean water level, respectively. The covariance matrix for the bending moments is readily computed from the information in Table 1.

Figure 5 shows a comparison between the ß-index values of the three alternatives for different prestress levels when only wave loading is considered. The dotted lines indicate maximum attainable indices for the serviceability limit state. The results presented in Figure 6 are computed for the case when also other loads are included. These loads are represented by additional expectation values, variances and covariances, and the new total expectation value and variance of M_y will be:

$$\mu_{M_y} = \mu^W_{M_y} + \mu^A_{M_y} = \mu^A_{M_y}$$

$$\sigma^2_{M_y} = (\sigma^2_{M_y})^W + (\sigma^2_{M_y})^A + 2\ \mathrm{cov}(M^W_y\ M^A_y) \qquad (27)$$

where superscript W denotes sea waves and superscript A denotes additional loads due to traffic, wind, snow and water current. In a short term analysis it is reasonable to put the covariances between the moments due to waves and other loads equal to zero, and as shown in Reference /20/, the last equation above then becomes:

$$\sigma^2_{M_y} = (\sigma^2_{M_y})^W + (\sigma^2_{M_y})^A \qquad (28)$$

Similar equations hold for M_z, and the covariance between M_y and M_z is simply expressed as

$$\mathrm{cov}(M_y\ M_z) = \mathrm{cov}(M^W_y\ M^W_z) \qquad (29)$$

under the assumption made above. The applied numerical values for the additional loads are believed to be representative, /14/. The choice of realistic magnitudes for the coefficients of variation is more difficult, on the other hand. The effect of varying these coefficients is closer described in Reference /20/.

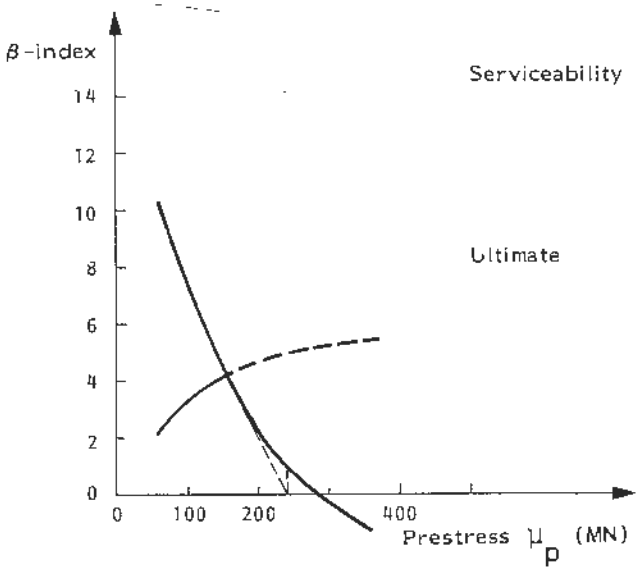

μ_p	β-index
60	2.14
110	3.42
180	4.42
240	4.87
360	5.30
60	10.24
110	6.96
180	3.17
240	1.03
360	-1.39

Alternative 1

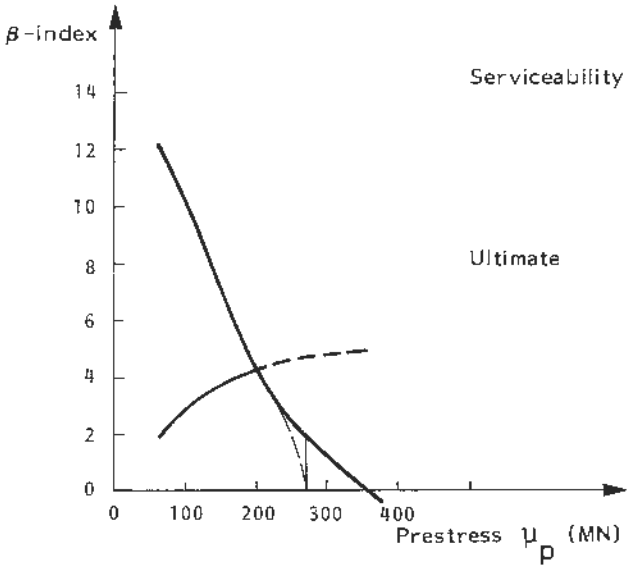

μ_p	β-index
60	1.88
110	3.05
180	4.04
240	4.51
360	4.97
60	12.10
110	9.40
180	5.32
240	2.80
360	-0.14

Alternative 2

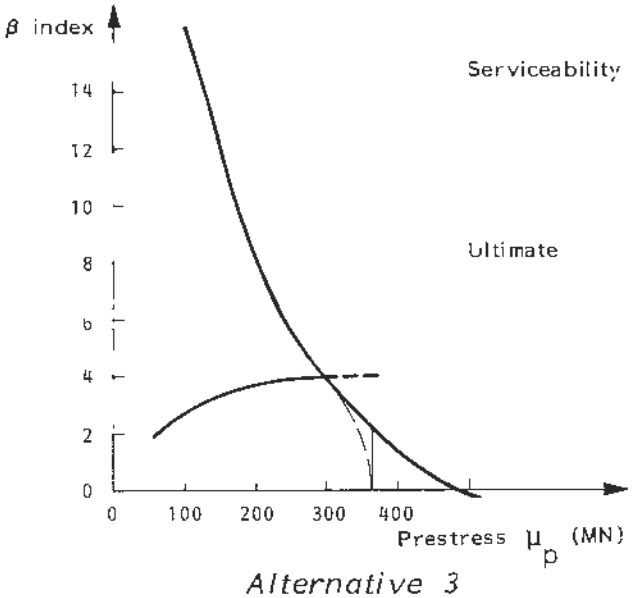

μ_p	β-index
60	1.99
110	2.96
180	3.62
240	3.87
360	4.09
60	20.35
110	15.44
180	9.50
240	6.07
360	2.13
470	0.15
561	-0.86

Alternative 3

Figure 5 β-index as function of prestress exeptation value. Wave load acting alone

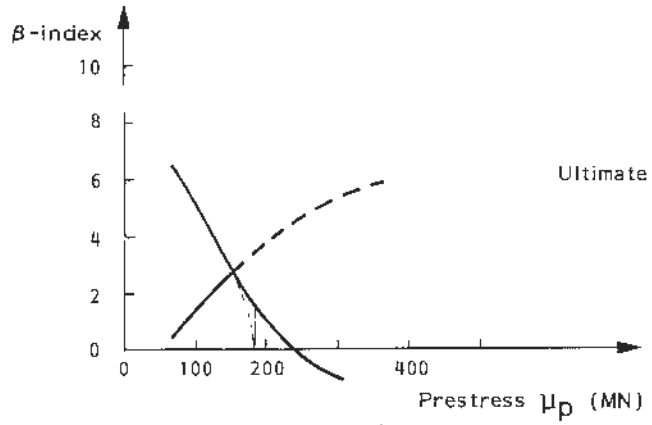

μp	β-index
60	0.45
110	1.90
180	3.48
240	4.52
360	5.88
60	6.46
110	4.38
180	1.60
240	-0.09
360	-1.81

Alternative 1

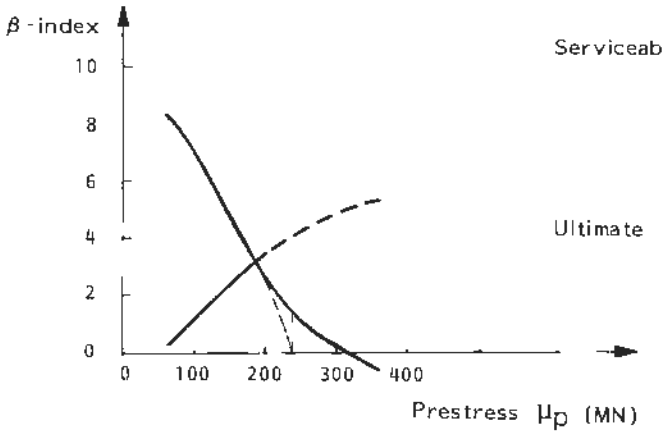

μp	β-index
60	0.30
110	1.58
180	3.05
240	4.03
360	5.34
60	8.32
110	6.58
180	3.67
240	1.40
360	0.70

Alternative 2

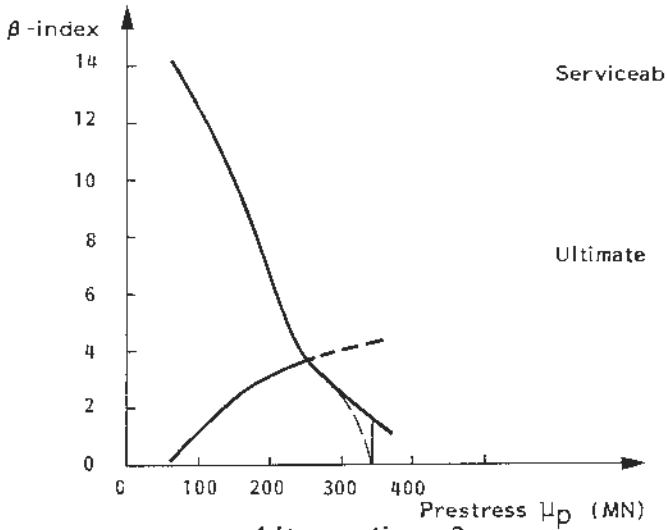

μp	β-index
60	0.17
110	1.46
180	2.76
240	3.50
360	4.37
60	14.11
110	11.62
180	8.30
240	3.94
360	1.06

Alternative 3

μ_N^A = 11.7 MN	$\mu_{M_y}^A$ = 53.9 MNm	$\mu_{M_z}^A$ = 176 MNm
σ_N^A = 4.7 MN	$\sigma_{M_y}^A$ = 21.5 MNm	$\sigma_{M_z}^A$ = 70.6 MNm

Figure 6 β-index as function of prestress expectation value. Additional loads included

The curves in Figures 5 and 6 reveal one quite surprising phenomenon: The lightest design alternative (no. 1) exhibits largest safety indices against serviceability failure. The indices corresponding to ultimate failure, however, are significantly reduced for this alternative as compared to the two others. For design alternatives two and three it is thus possible to increase the safety index level above 2.0 for the serviceability limit state and 5.0 for the ultimate limit state at the same time, by a proper choice of the prestress. This also holds when additional loads are included.

It is clearly seen that inclusion of these additional loads disfavours the lightest design alternative. Still it may be considered a safe design if the prestress is chosen so as to make the indices larger than the rule-of-thumb values 1.0 and 3.0 simultaneously for the two different limit states.

Definite conclusions about the reliability of the designs, however, must be based on level 3 studies. Such a study has been carried out for the first design alternative by means of the theory outlined in Section 4.2 above. The results are depicted in Figures 7 and 8 for sea state durations of 2 hrs and 4 hrs, respectively. Two sets of variances for the prestressing force are applied. The first set corresponds to no correlation between the forces in cables below and above the sea surface, and the second set corresponds to full correlation. The quantities μ_p and σ_p in the figures denote the expectation value and standard deviation of the prestressing force, respectively.

Suggestive target values for the probability of failure may be found in Table 2 below. The values of p_f correspond to a common design practice for simple scalar Gaussian processes: The design load is taken as the expected largest maximum load multiplied by a partial coefficient γ. Frequently γ is taken as 1.0 for the serviceability limit and 1.3 for the ultimate limit state when the wave load is acting simultaneously with other loads. The values below are equal to the probability of the largest maximum exceeding this design load in the given time period.

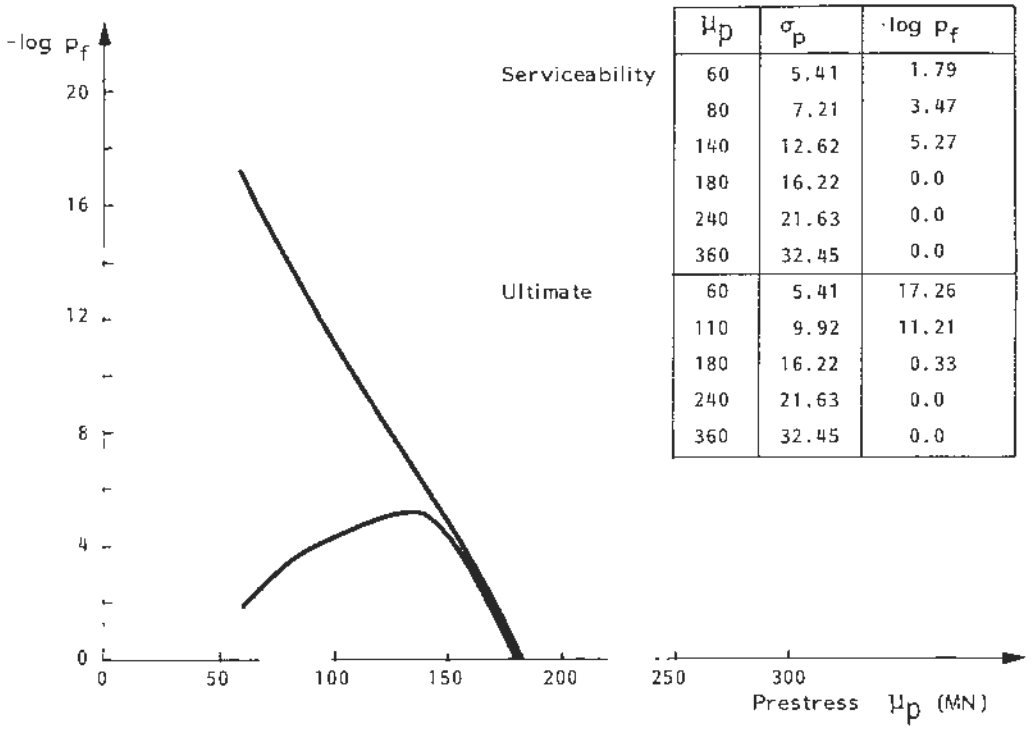

	μ_p	σ_p	-log p_f
Serviceability	60	5.41	1.79
	80	7.21	3.47
	140	12.62	5.27
	180	16.22	0.0
	240	21.63	0.0
	360	32.45	0.0
Ultimate	60	5.41	17.26
	110	9.92	11.21
	180	16.22	0.33
	240	21.63	0.0
	360	32.45	0.0

(a) Uncorrelated prestressing force in upper and lower cables

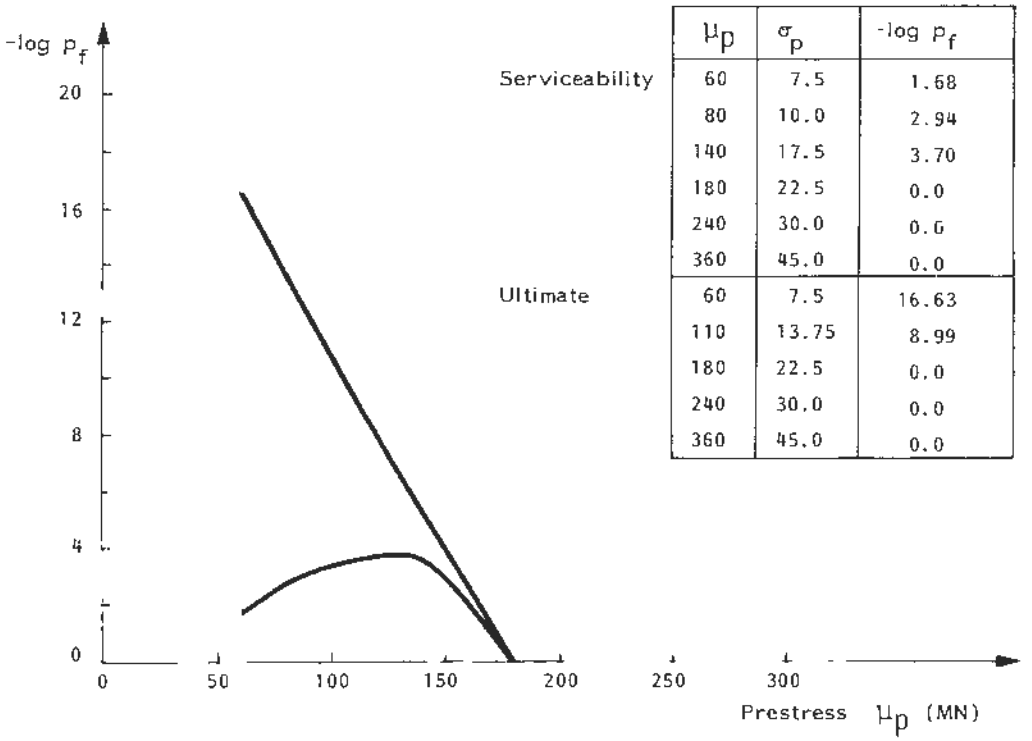

	μ_p	σ_p	-log p_f
Serviceability	60	7.5	1.68
	80	10.0	2.94
	140	17.5	3.70
	180	22.5	0.0
	240	30.0	0.0
	360	45.0	0.0
Ultimate	60	7.5	16.63
	110	13.75	8.99
	180	22.5	0.0
	240	30.0	0.0
	360	45.0	0.0

(b) Fully correlated prestressing force in cables

Figure 7 Probability of failure as function of prestress expectation value. Alternative 1, wave load acting alone. Storm duration: 2 hrs.

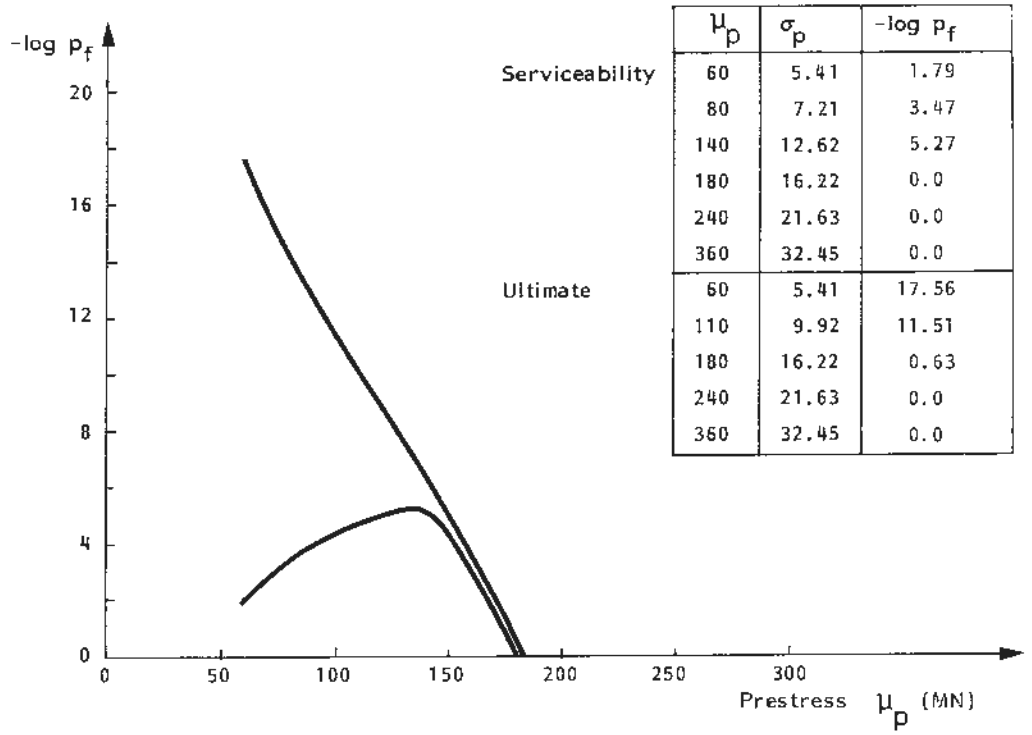

	μ_p	σ_p	-log p_f
Serviceability	60	5.41	1.79
	80	7.21	3.47
	140	12.62	5.27
	180	16.22	0.0
	240	21.63	0.0
	360	32.45	0.0
Ultimate	60	5.41	17.56
	110	9.92	11.51
	180	16.22	0.63
	240	21.63	0.0
	360	32.45	0.0

(a) Uncorrelated prestressing force in upper and lower cables

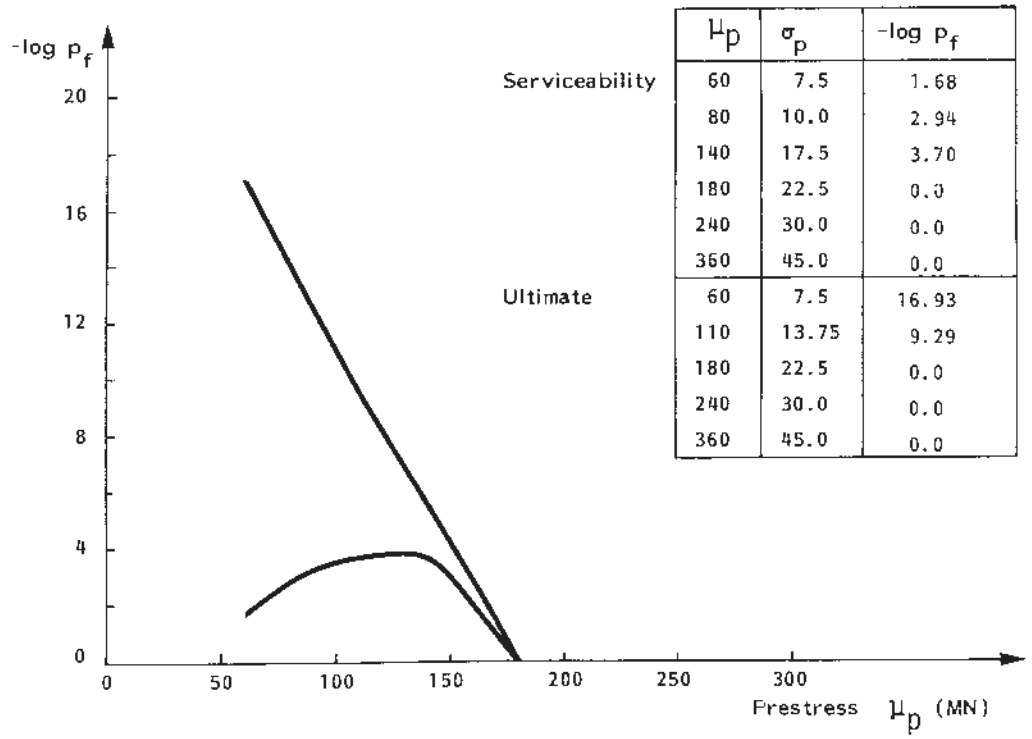

	μ_p	σ_p	-log p_f
Serviceability	60	7.5	1.68
	80	10.0	2.94
	140	17.5	3.70
	180	22.5	0.0
	240	30.0	0.0
	360	45.0	0.0
Ultimate	60	7.5	16.93
	110	13.75	9.29
	180	22.5	0.0
	240	30.0	0.0
	360	45.0	0.0

(b) Fully correlated prestressing force in cables

Figure 8 Probability of failure as function of prestress expectation value. Alternative 1, wave load acting alone. Storm duration: 4 hrs

Table 2 Suggestive target values for p_f

γ	Duration = 2 hrs Upcrossing rate = 0.20		Duration = 4 hrs Upcrossing rate = 0.20	
	p_f	$-\log p_f$	p_f	$-\log p_f$
1.00	0.450	0.347	0.449	0.348
1.25	$0.748 \cdot 10^{-2}$	2.126	$0.503 \cdot 10^{-2}$	2.300
1.50	$0.355 \cdot 10^{-4}$	4.450	$0.148 \cdot 10^{-4}$	4.830

It can be concluded that for the limit states considered, a sufficiently high reliability level can be achieved by a proper selection of prestressing force even for a storm duration of 4 hrs. It is important, however, that the optimal prestress interval is found to be more narrow than indicated by the β-index results. It is also observed that the effect of full correlation between prestressing forces is an increase of the probability of failure with up to two orders of magnitude.

7. CONCLUSIONS

Two different methods for the evaluation of the safety level of a floating bridge are applied for two specific collapse modes. Three design alternatives are compared in a simplified manner by means of the β-index. It is found that the "heaviest" design will tend to be the safest one when both wave loading and additional loads are included. A level 3 study, however, indicates that also the reliability level of the "lightest" alternative is satisfactory. It is also found that the representation of the wave loading as a stochastic process yields more narrow optimal prestress intervals than suggested by a β-index procedure.

As an extension of the work herein, a complete comparison of the designs should be carried out on a level 3 basis. The additional loads must then be represented by proper load models. Such refined analyses, however, should be based upon measured data. The results from the in-situ wave measurement program may then conveniently be incorporated, and the lifetime reliability of a specified design can be evaluated.

ACKNOWLEDGEMENTS

The work has to a large extent been carried out as part of a project supported by NTNF and the Norwegian Public Roads Administration. The authors are especially grateful for the support provided by H.T. Øderud from the latter institution.

REFERENCES

1. Om bru over Salhusfjorden. Stortingsmelding nr. 75, 1979-809. Ministry of Transport, Oslo, May 1980.

2. Andrew, C.E.: "A Floating Highway Bridge 6.470 Feet Long", Civil Engineering, Dec. 1959.

3. Hood Canal Floating Bridge: Phase I Report. Determination of the Causes of Failure, Tokola Offshore, Portland and Earl and Wright consulting engineers, San Francisco, Aug. 1979.

4. Hartz, B.J.: "Dynamic Analysis of the Hood Canal Floating Bridge Failure, in Structural Safety and Reliability, edited by T. Moan and M. Shinozuka, Elsvier, Amsterdam, 1981.

5. Mukherji, B.: Dynamic Behaviour of a Continuous Floating Bridge, Ph.D. Dissertation, University of Washington, Seattle, 1972.

6. Hartz, B.J. and Mukherji, B.: "Dynamic Response of a Floating Bridge to Wave Forces", International Conference on Bridging Rion-Antirrion, Patras, Greece, 1977.

7. Holand, I., Langen, I. and Sigbjörnsson, R.: Dynamic Analysis of a Curved Floating Bridge, IABSE Proceedings P-5/77, 1977.

8. Clough, D., Sigbjörnsson, R. and Remseth, S.N.: Response of a Submerged, Buoyant Tubular Bridge Subjected to Irregular Sea Waves, SINTEF Report STF71 A77028, Trondheim, 1977.

9. Langen, I. and Sigbjörnsson, R.: "On stochastic dynamics of floating bridges", Engineering Structures, Vol. 2, No. 4, 1980, pp. 209-216.

10. Georgiadis, C.: Wave Induced Vibrations of Continuous Floating Structures, Ph.D. Dissertation, University of Washington, Seattle, 1981.

11. Adee, B.H. and Martin, W.: "Theoretical Analysis of Floating Breakwater Performance", in 1974 Floating Breakwaters Conference Papers, University of Rhode Island, Marine Technical Report Series Number 24, 1974, pp. 21-39.

12. Wen, Y-K.: "Interaction of Ocean Waves with Floating Plate", J. Eng. Mech. Div. ASCE, 100, EM2, 375-395.

13. Sigbjörnsson, R.: "Towards Probabilistic Design of Floating Bridges", SINTEF Report STF71 A80010, Trondheim, 1980.

14. Øderud, H.T.: "Beregninger for Salhus flytebro", Handwritten notes, Vegdirektoratet, Oslo, Undated.

15. Langen, I.: "Probabilistic Methods for Dynamic Analysis of Floating Bridges", Norwegian Maritime Research, No. 1, 1983. Also published as SINTEF Report STF71 A81013, 1981.

16. Langen, I.: "On Dynamic Analysis of Floating Bridges", Report 81-1, Division of Structural Mechanics, The Norwegian Institute of Technology, Trondheim, 1981.

17. Hasofer, A.M. and Lind, N.C.: "An exact and Invariant First-order Reliability Format", J. of the Engineering Mechanics Division, ASCE, Vol. 100, No. EM1, 1974.

18. Thoft-Christensen, R. and Baker, M.J.: "Structural Reliability Theory and its Applications", Springer Verlag, 1982.

19. Leira, B.J.: "Probabilistic Design - A Literature Survey", SINTEF Report STF71 A83020, Trondheim, 1983.

20. Leira, B.J.: "Probabilistic Design - An Application to Floating Bridges", SINTEF Report STF71 A83024, Trondheim, 1983.

21. Belyaev, Y.K.: "On the Number of Exits Across the Boundary of a Region by a Vector Stochastic Process", Theory of Probability Applications, Vol. 13, 1968.

22. Bolotin, V.V.: "Application of the Methods of the Theory of Probability and Theory of Reliability to Analysis of Structures", Air Force Systems Command, U.S.A., 1974.

23. Veneziano, D. et al.: "Vector-process Models for System Reliability", J. of the Engineering Mechanics Division, ASCE, Vol. 103, No. EM3, 1977.

24. Leira, B.J.: "Probabilistic Design - A Level 3 Study", SINTEF Report to appear.

25. Skjerven, E.J.: "Probabilistiske Metodar for Undersøkelse av Konstruksjonars Påliteligheit", Diploma thesis in Norwegian, Division of Structural Mechanics, The Norwegian Institute of Technology, Trondheim,1982.

26. NS 3473: "Concrete Structures. Design Rules". Norges Byggstandardiseringsråd, September, 1973.

27. Øderud, H.T.: "Kapasitet av Kassetverrsnitt utsatt for Normalkraft og Bøyning om to Akser", Handwritten notes, Vegdirektoratet, Oslo, undated.

28. Johnson, W. and Reiss, R.D.: "Numerical Analysis", Addison-Wesley, 1982.

29. Øderud, H.T.: "Salhus flytebro, tegning nr. 523/78 av pontong armering", Statens Vegvesen, Oslo, 1978.